Supplementary Information

for

Four-Step Electron Transfer Coupled Spin Transition

in a Cyano-bridged [Fe$_2$Co$_2$] Square Complex

Taisuke Ikeda,[a] Yu-Bo Huang,[a] Shu-Qi Wu,[a] Wenwei Zheng,[a] Wen-Huang Xu,[a] Xiaopeng Zhang,[a] Tianchi Ji,[a] Mikoto Uematsu,[a] Shinji Kanegawa,[a] Sheng-Qun Su*[a] and Osamu Sato*[a]

a. Institute for Materials Chemistry and Engineering and IRCCS, Kyushu University, 744 Motooka, Nishi-ku, Fukuoka 819-0395, Japan.

Experimental methods

Single crystal X-ray structure determination

A block crystal was coated with oil-based cryoprotectant and fixed on nylon loop. Diffraction data was collected at 100 K with XtaLAB Synergy-R/DW (Rigaku) using Mo-Kα radiation ($\lambda = 0.71073$ Å) under cold nitrogen gas flow. The structure was solved by direct method and refined by full-matrix least-squared on F^2 with SHELX program[1] introduced on Olex2 program[2]. All non-hydrogen atoms were treated with anisotropic thermal parameters. Hydrogen atoms were geometrically added and refined by riding model. Supplementary crystallographic data can be obtained free of charge from the Cambridge Crystallographic Data Center via www.ccdc.cam.ac.uk/data_request/cif. (CCDC number: 2337773)

Magnetometry

DC magnetometry was performed with MPMS-5S SQUID magnetometer in the magnetic field of 5000 Oe at 5–400 K. Well-ground microcrystalline sample was put in gelatine capsule, which was fixed into a plastic straw attached on a sample rod except the photo-magnetometry. In the photo-magnetometry, well-ground sample was pasted on the transparent tape and fixed on a plastic straw with Pd rod, then, the straw was attached on a sample rod. The Nd-YAG laser (HPC/GLMP-0200A, 532 nm, cw) was used as light source, which was irradiated for 2 h before the measurement. All measured data were corrected by diamagnetic contribution. Pd contribution was also removed from photo-magnetic data. In the analysis of **1**, the paramagnetic fractions were estimated as that all (100%) of the [Fe$_2$Co$_2$] units are paramagnetic state in the high-temperature (HT) phase (over 360 K), and the paramagnetic fractions in the intermediate phases were calculated from proportional comparison of their $\chi_M T$ values with the HT phase.

Variable-temperature IR spectroscopy

Variable-temperature IR absorption spectrum was measured with FT-IR spectrophotometer (FT/IR-660Plus, JASCO), cryostat (LT-3-110, Advanced Research Systems) at 80–300 K and heating stage (HCS402, INSTEC) at 400 K. Ground sample was put betweenn grained and plane CaF$_2$ plates as thin layer. In the measurement of **1**, the spectrum was firstly measured at 400 K, which is enough high temperature for the complete desolvation. Subsequently, hot sample with CaF$_2$ plates was quickly inserted in the cryostat and placed in vacuum so as not to absorb water from the ambient air. Finally, the spectrums of **1** were measured at 80–300 K.

Powder X-ray diffraction (PXRD) analysis

Powder X-ray diffractions were measured with TTR-III (Rigaku) using Cu-Kα radiation ($\lambda = 1.54056$ Å). Samples were attached on a silicon stage and the diffraction patterns were recorded with the scan

rate of 2°/min at room temperature. During the measurement of **1**·8EtOH, the sample was covered with grease (Apiezon N, M&I Materials) to prevent the removal of the crystal solvent.

Thermogravimetric analysis (TGA)

TGA was performed with integrated thermal analysis system (TG/DTA6300, Seiko Instruments Inc.). Polycrystalline samples were heated from 300 K to 520 K with the sweeping rate of 10 K min^{-1} in the air.

Variable temperature UV-vis spectroscopy

Variable-temperature UV-vis absorption spectrum was measured with UV-vis spectrophotometer (UV-3100PC, Shimadzu). Well-ground sample was attached between transparent tapes as thin layer, then sandwiched with plane CaF$_2$ plates. The temperature was controlled with cryostat (Nagase Techno Engineering) at 80–300 K and heating stage (HCS402, INSTEC) at 400 K respectively. The measurement was carried out as well as variable-temperature IR spectroscopy to prevent the absorption of water.

Synthesis
Chemical reagents

All chemical reagents were purchased from FUJIFILM Wako Pure Chemical Corporation, Tokyo Chemical Industry Co., Ltd. and Sigma-Aldrich company. They were used without further purification.

N, N'-Bis(4-methylbenzyl)-*N, N*'-bis(pyridin-2-ylmethyl)ethane-1,2-diamine (L) and [NBu$_4$][Fe(Tp)(CN)$_3$] were synthesized according to the literature method with slight modification[3,4].

{[Fe(Tp)(CN)$_3$]$_2$[Co(L)]$_2$}(ClO$_4$)$_2$·8EtOH (1·8EtOH) Synthesis

Co(ClO$_4$)$_2$·6H$_2$O (110 mg, 300 μmol) and L (135 mg, 300 μmol) were reacted in ethanol (25 ml) with stirring for 10 min. Subsequently, [NBu$_4$][Fe(Tp)(CN)$_3$] (177 mg, 300 μmol) was added into the reaction mixture. After the solution was stirred for 5 min, green powder was removed via filtration. Resulted filtrate was kept in 60°C for 1 day to obtain green plate crystal. (Yield: 128 mg, 19 %)

{[Fe(Tp)(CN)$_3$]$_2$[Co(L)]$_2$}(ClO$_4$)$_2$ (1) Synthesis

The crystal of **1**·8EtOH was heated at 400 K in nitrogen atmosphere for 1 h to obtain reddish brown crystal.

Elemental analysis Found: C, 52.49; H, 4.65; N, 18.91. Calc. for C$_{84}$H$_{88}$Fe$_2$Co$_2$B$_2$N$_{26}$O$_8$Cl$_2$: C, 52.77; H, 4.64; N, 19.05%

{[Fe(Tp)(CN)₃]₂[Co(L)]₂}(ClO₄)₂·3H₂O (1·3H₂O) Synthesis

The crystal of **1** was kept in the air overnight to obtain brown crystal.

Elemental analysis Found: C, 51.47; H, 4.84; N, 18.37. Calc. for $C_{84}H_{94}Fe_2Co_2B_2N_{26}O_{11}Cl_2$: C, 51.32; H, 4.82; N, 18.53%

Table S1. Crystallographic parameters of **1**·8EtOH

Temperature /K	100
Formula	$C_{50}H_{68}BClCoFeN_{13}O_8$
Formula Weight /g mol⁻¹	1140.21
Crystal Color	green
Crystal System	monoclinic
Space Group	$P2_1/n$
a /Å	16.5955(4)
b /Å	14.0531(3)
c /Å	23.5734(6)
α /°	90
β /°	98.168(2)
γ /°	90
V /Å³	5442.0(2)
Z	4
d_{calc} /g cm⁻³	1.392
R_{int}	0.0512
R_1[a] $(I > 2\sigma(I))$	0.0477
wR_2[b] (all data)	0.1335
CCDC number	2337773

a $R_1 = \Sigma||F_0|-|F_c|| / \Sigma|F_0|$, b $wR_2 = \{\Sigma[w(F_0^2 - F_c^2)^2] / \Sigma[w(F_0^2)^2]\}^{1/2}$
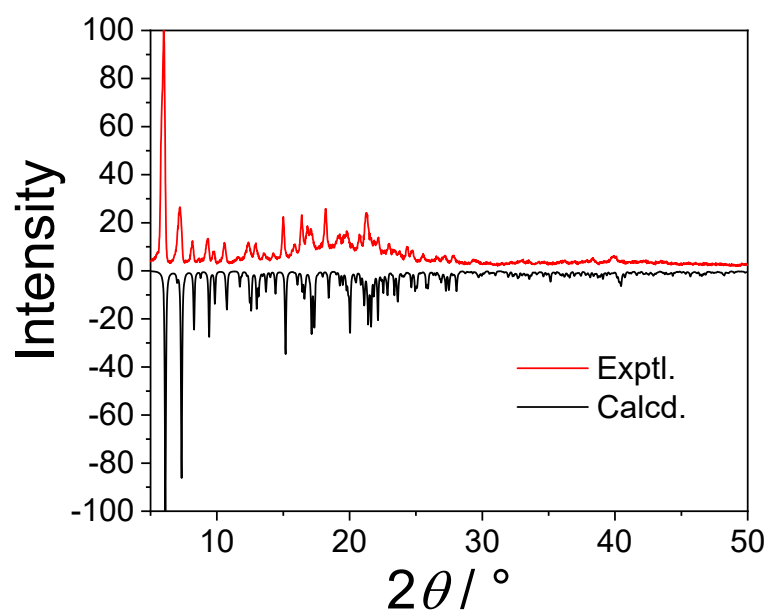
Fig. S1. PXRD pattern of **1**·8EtOH. The measured data (Exptl., red line) is well-consistent with the simulated pattern based on the single crystal X-ray diffraction analysis (Calcd., black line). This pattern supports the purity of the original form, **1**·8EtOH.
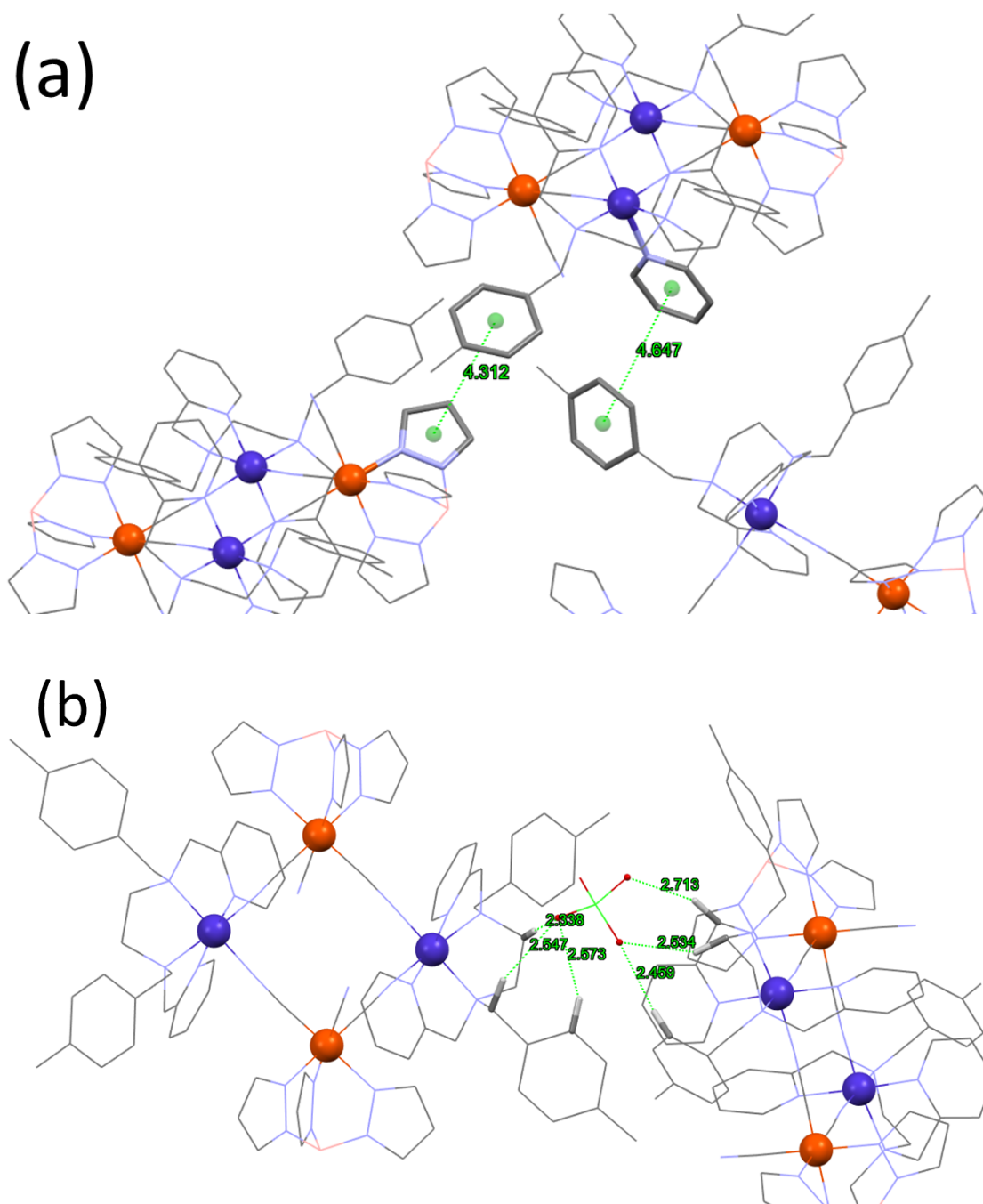
Fig. S2. Packing structure of **1**·8EtOH at 100 K. Counter ions and solvent molecules are fittingly omitted for clarity. (a)The distances of neighboring aromatic rings are 4.312 and 4.647 Å and (b) the distances of O atoms of perchlorate and H atoms surrounding them are 2.338–2.713 Å, which are not short enough for intermolecular π-π interaction or hydrogen bonding. However, they potentially provide meaningful intermolecular interaction to stabilize intermediate phases after desolvation due to the change of packing structure.
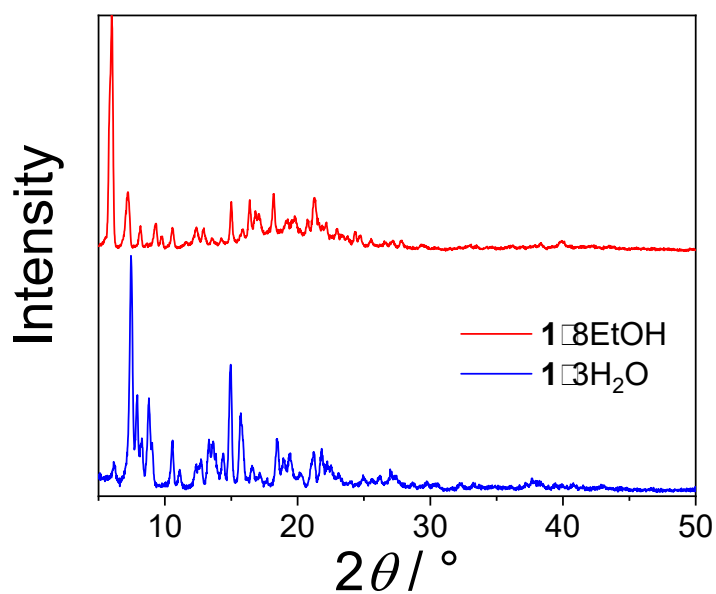
Fig. S3. PXRD pattern of **1**·8EtOH (red line) and **1**·3H$_2$O (blue line). This pattern change indicates the switch of the crystal structure and that crystalline character was kept through desolvation and solvation. However, PXRD pattern of **1** couldn't be obtained because of the instability of the desolvated form.
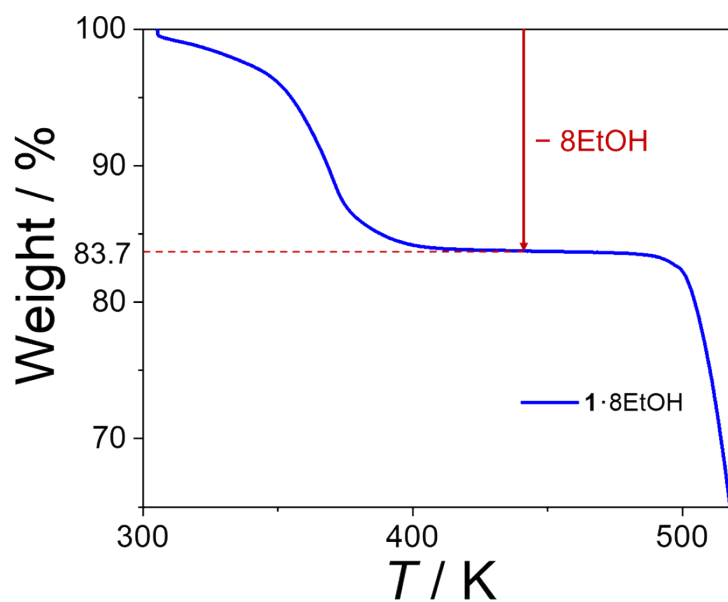

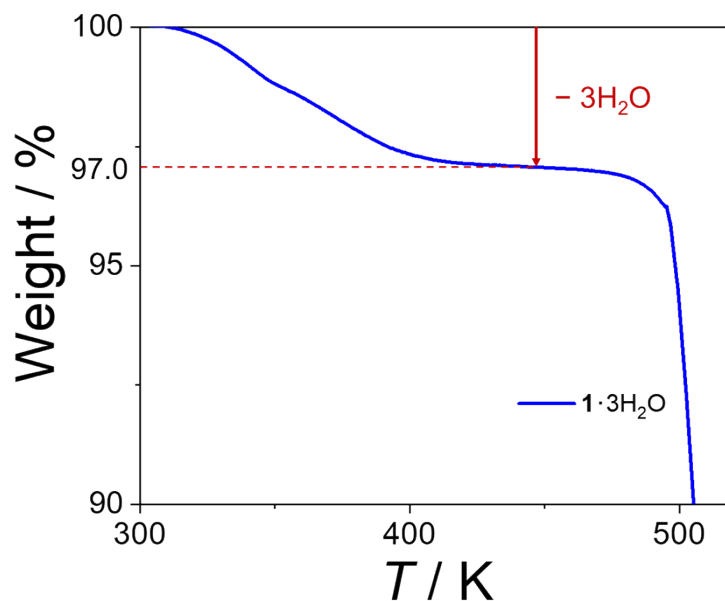Fig. S4. TGA of **1**·8EtOH. 16.3 % of the weight loss corresponds to the removal of eight ethanol molecules.

Fig. S5. TGA of **1**·3H$_2$O. 2.7 % of the weight loss corresponds to the removal of three water molecules.
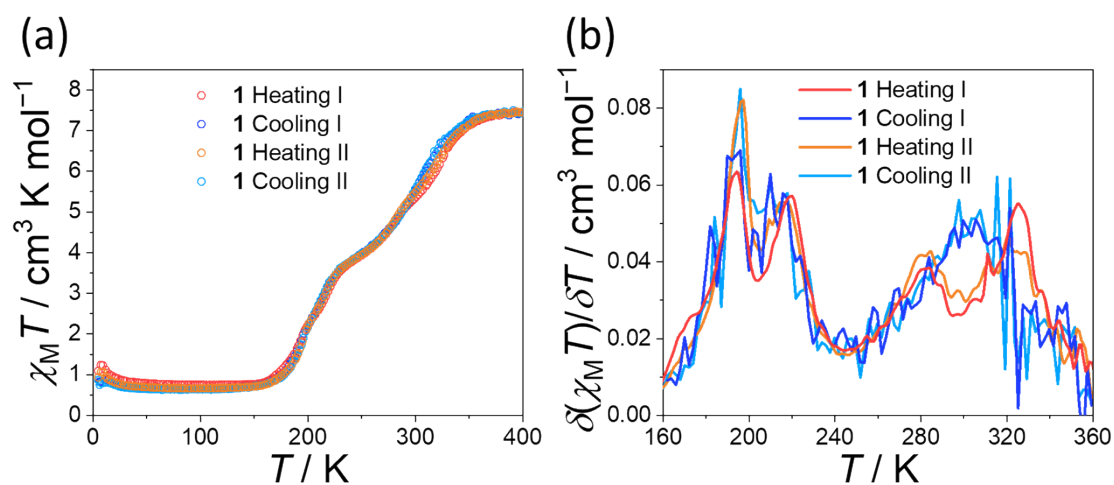

Fig. S6. (a) Magnetic susceptibility of **1** in two heating-cooling cycles. In a cycle, the sample was heated from 5 K to 400 K (red in the first cycle and orange in the second cycle) and subsequently cooled from 400 K to 5 K (blue in the first cycle and light blue in the second cycle). The sweeping rates were 5 K/min for all processes. (b) The first derivatives of the individual $\chi_M T$ vs. T curves of **1** in Fig. S6a. Although the peak at 280–330 K is broad and not clear in the cooling processes, four-step character was clearly observed in the heating processes and it was completely repeated even in the second cycle.
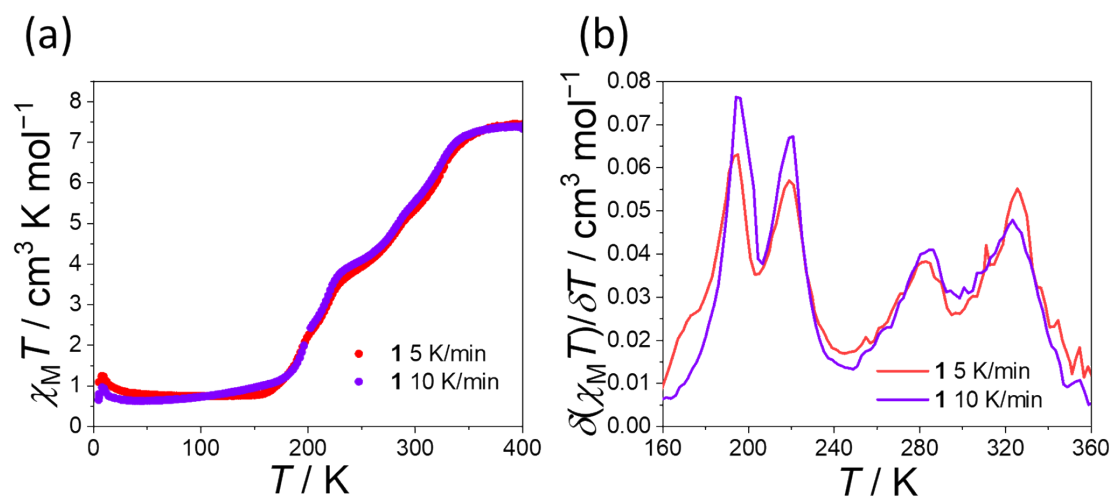
Fig. S7. (a) Magnetic susceptibility of **1** in the different sweeping rates of heating. Red plot represents 5 K/min and purple plot represents 10 K/min. (b) The first derivative of the $\chi_M T$ vs. T curve of **1** in Fig. 7a. Four-step character was observed in both sweeping rates.
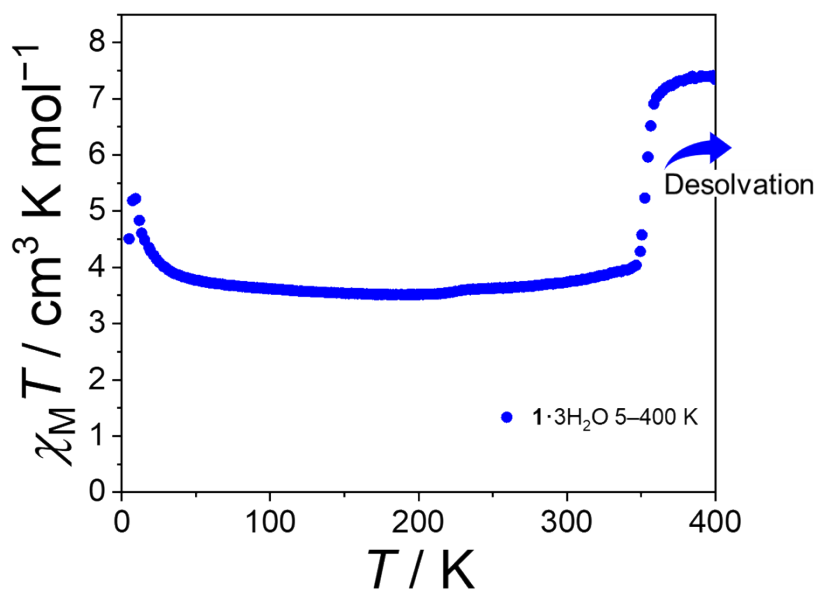

Fig. S8. Magnetic property of **1**·3H$_2$O. ETCST turned off by the solvation of 3H$_2$O. After heating over 370 K, the HT phase of desolvated **1** was recovered.

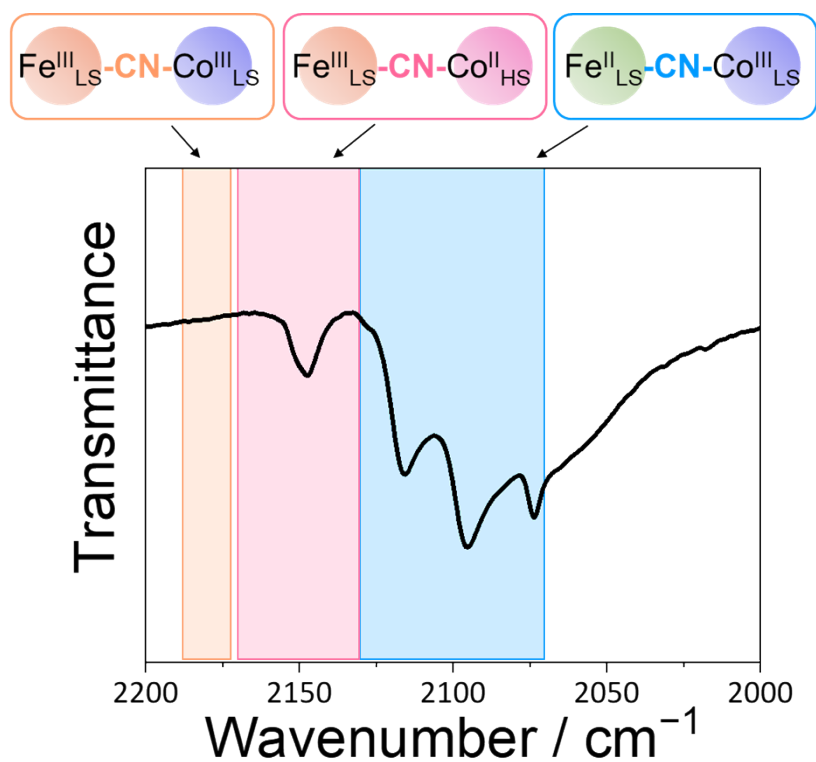Fig. S9. IR spectrum of **1**·3H$_2$O at 300 K. The absorption at 2070–2130 cm^{-1} and 2130–2170 cm^{-1} indicate existence of both [Fe$^{II}_{LS}$Co$^{III}_{LS}$] and [Fe$^{III}_{LS}$Co$^{II}_{HS}$] structures.
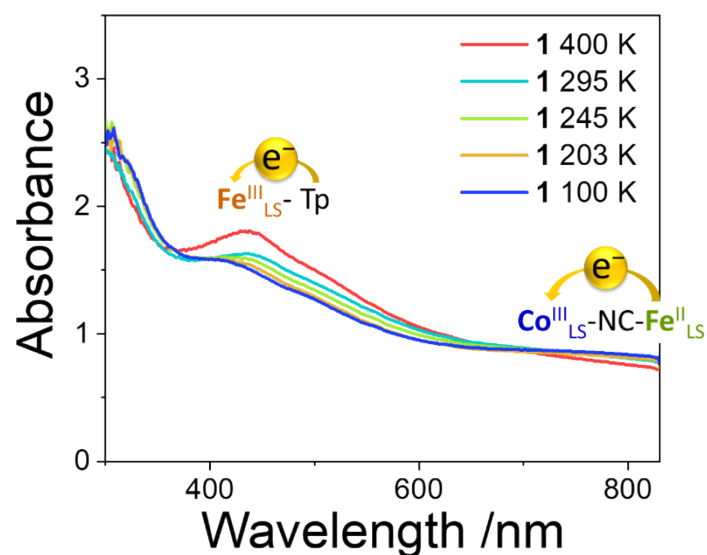

Figure S10. Variable temperature UV-vis spectrum of **1**. Absorption band around 730 nm and 430 nm correspond to metal to metal charge transfer (MMCT) from Fe$^{II}_{LS}$ to Co$^{III}_{LS}$ and ligand to metal charge transfer (LMCT) from Tp to Fe$^{III}_{LS}$ respectively[5–10]. During heating process, peak intensity at 430 nm

was increased while the one at 730 nm was decreased. These spectral change support thermal induced charge transfer.

References

[1] G. M. Sheldrick, *Acta Cryst.*, 2015, **C71**, 3–8

[2] O. V. Dolomanov, L. J. Bourhis, R. J. Gildea, J. A. K. Howard and H. Puschmann, *Appl.Cryst.*, 2009, **42**, 339–341

[3] J. R. Aldrich-Wright, R. F. Fenton, P. Leverett, F. S. Stephens, P. A. Williams and R. S. Vagg, *J. Coord. Chem.*, 2007, **60**, 2015–2034

[4] S. Wang, J.-L. Zuo, H.-C. Zhou, Y. Song and X.-Z. You, *Inorg. Chim. Acta*, 2005, **358**, 2101–2106

[5] Y. Zhang, D. Li, R. Cl*é*rac, M. Kalisz, C. Mathoni*è*re, and S. M. Holmes, *Angew. Chem. Int. Ed.*, 2010, **49**, 3752–3756

[6] M. Nihei, Y. Sekine, N. Suganami, K. Nakazawa, A. Nakano, H. Nakao, Y. Murakami and H. Oshio, *J. Am. Chem. Soc.*, 2011, **133**, 3592–3600

[7] C. Zheng, J. Xu, Z. Yang, J. Tao and D. Li, *Inorg. Chem.*, 2015, **54**, 9687−9689

[8] C.-Q. Jiao, Y.-S. Meng, Y. Yu, W.-J. Jiang, W. Wen, H. Oshio, Y. Luo, C.-Y. Duan and T. Liu, *Angew. Chem. Int. Ed*., 2019, **58**, 17009–17015

[9] J. Yadav, D. J. Mondal and S. Konar, *Chem. Commun.*, 2021, **57**, 5925–5928

[10] L. Meng, Y.-F. Deng, J. Liu, Y. J. Liu and Y.-Z. Zhang, *Dalton Trans.*, 2022, **51**, 15669–15674